PCCP

PAPER

Cite this: *Phys. Chem. Chem. Phys.*, 2016, **18**, 23538

Direct phase coexistence molecular dynamics study of the phase equilibria of the ternary methane–carbon dioxide–water hydrate system

Vasileios K. Michalis,[a] Ioannis N. Tsimpanogiannis,[b] Athanassios K. Stubos[b] and Ioannis G. Economou*[a]

Received 4th July 2016,
Accepted 26th July 2016

DOI: 10.1039/c6cp04647a

www.rsc.org/pccp

Molecular dynamics simulation is used to predict the phase equilibrium conditions of a ternary hydrate system. In particular, the direct phase coexistence methodology is implemented for the determination of the three-phase coexistence temperature of the methane–carbon dioxide–water hydrate system at elevated pressures. The TIP4P/ice, TraPPE-UA and OPLS-UA forcefields for water, carbon dioxide and methane respectively are used, in line with our previous studies of the phase equilibria of the corresponding binary hydrate systems. The solubility in the aqueous phase of the guest molecules of the respective binary and ternary systems is examined under hydrate-forming conditions, providing insight into the predictive capability of the methodology as well as the combination of these forcefields to accurately describe the phase behavior of the ternary system. The three-phase coexistence temperature is calculated at 400, 1000 and 2000 bar for two compositions of the methane–carbon dioxide mixture. The predicted values are compared with available calculations with satisfactory agreement. An estimation is also provided for the fraction of the guest molecules in the mixed hydrate phase under the conditions examined.

1. Introduction

Clathrate hydrates are characterized as inclusion compounds consisting of water and guest molecules of appropriate size.[1] The guest molecules are enclathrated in hydrogen-bonded cages of water molecules, forming a crystal lattice. The stability as well as the type of the hydrate structure depends on the particular interactions of the guest molecules with water. More than 130 guest molecules, or hydrate-formers as they are routinely called, have been identified such as methane, ethane, propane, nitrogen, carbon dioxide, and hydrogen, which are of particular industrial interest. The most common hydrate lattice structures are sI, sII and sH, which mainly differ by the type of the cages that they consist of as well as the ratio of cages of different type. For example, both methane and carbon dioxide mainly form sI hydrates,[2] whose unit cell consists of two dodecahedra (5^{12}) and six larger tetradecahedra ($5^{12}6^2$) water cages.

Hydrates have been studied extensively due to their scientific and engineering interest. Natural gas hydrates, in particular, are important to the oil and gas industry, primarily related to flow assurance[3,4] and secondarily as a potential energy source due to the fact that they are geologically abundant, located mainly under the oceanic floor and the permafrost regions of the planet.[5] Furthermore, hydrates have drawn interest for gas storage[6,7] and separation applications,[8] as well as due to their environmental[9] and geological importance.[10,11]

Apart from the traditional methods for the study of hydrate systems, which include experimental[1,12] and equation of state approaches,[13–15] molecular dynamics (MD) simulation[16] is increasingly proving its usefulness, as it can provide insightful molecular level information and can also be used for the estimation of hydrate properties in the absence of experimental data.[17] Naturally, a first necessary step towards this goal is the verification of the validity of the used methodologies and forcefields by comparing the results of MD with available experimental data.

The scope of the present study is the extension of our previous works on the calculation of three-phase equilibrium conditions of pure methane[18] and pure carbon dioxide[19] hydrates, to the respective ternary mixture (methane–carbon dioxide–water). In both previous studies, we have implemented the direct phase coexistence methodology,[20] where a solid hydrate phase is placed in direct contact with an aqueous phase and a guest-rich phase. Given that these systems have one intensive degree of freedom, by fixing the pressure for example, one can perform simulations at different temperatures and by monitoring the tendency of the system to move towards either hydrate growth or hydrate dissociation, the equilibrium temperature can be estimated. It has

[a] *Chemical Engineering Program, Texas A&M University at Qatar, PO Box 23874, Doha, Qatar. E-mail: ioannis.economou@qatar.tamu.edu*
[b] *Environmental Research Laboratory, National Center for Scientific Research "Demokritos", GR-15310 Aghia Paraskevi Attikis, Greece*

been shown[18,21] that within the length and time scales studied, such kind of systems exhibit stochastic behavior close to equilibrium conditions and thus necessitate a statistical averaging of the results in order to achieve consistent predictions. Additionally, the importance of the molecular models involved cannot be underestimated. It was shown that both water–water and water–guest interactions affect the predicted equilibrium conditions. In particular, in line with the work of Vega and coworkers[22,23] we have shown[18,19] that it is advantageous to use the TIP4P/ice water forcefield[24] as its good performance at predicting the melting temperature of ice[25] is also reflected in the prediction of the hydrate equilibrium conditions. Regarding the water–guest interactions, we have shown for both systems examined previously, that the ability of the guest forcefield to provide accurate predictions of the guest solubility in the liquid water-rich phase is of critical importance. For the case of the OPLS-UA methane model[26] the predictions of solubility under hydrate forming conditions are quite accurate.[27] On the other hand, it was found that for the case of the TraPPE-UA model[28] for carbon dioxide, a modification in the water–carbon dioxide energy cross-interaction parameter between the oxygens of unlike molecules was necessary in order to correct the predicted solubility of carbon dioxide in water, and thus improve in turn the predictions of the three-phase equilibrium conditions of the hydrate system.[19]

There is only a small number of molecular simulation works that have studied the methane–carbon dioxide–water hydrate system (*i.e.*, MD,[29–35] DFT,[36–38] and Monte Carlo simulations[39]). Most of the MD studies[31–35] focused primarily on the examination of the replacement of methane with carbon dioxide in the hydrate structure.[40] A detailed review of the issue is provided by Komatsu *et al.*[41] On the other hand, the MD works of Yi *et al.*[29] focused on the hydrate growth rate and dissociation[30] of the ternary system.

Experimentally, the three-phase equilibrium conditions for the particular ternary system have been measured extensively for pressures below 100 bar, while a limited amount of experimental measurements are available in the pressure range of 100 to 200 bar. On the other hand, no experimental data, to the best of our knowledge, exist for pressures higher than 200 bar. An extensive review of earlier experimental studies can be found in Sloan and Koh,[1] as well as at the NIST hydrate database,[42] while more recent experimental data can be found in ref. 43–51. Furthermore, Eslamimanesh *et al.*[52,53] presented a detailed discussion regarding the experimental data assessment.

Limited is also the number of experimental studies regarding the solubility of carbon dioxide and methane in the water-rich phase of the ternary system at vapor–liquid equilibrium (VLE). Notably, Qin *et al.*[54] carried out experimental measurements on VLE in the ternary systems at temperatures from 324 up to 375 K and pressures in the range of 100 to 500 bar for three different compositions. Ghafri *et al.*[51] also reported measurements both at VLLE at temperatures from 285.15 to 303.5 K and pressures up to the upper critical end point, and at VLE from 323.15 to 423.15 K and up to 200 bar for an equimolar carbon dioxide to methane composition. Lobanova *et al.*[55] reported experimental measurements at 393.15 K and pressures in the range of 60 to 120 bar,

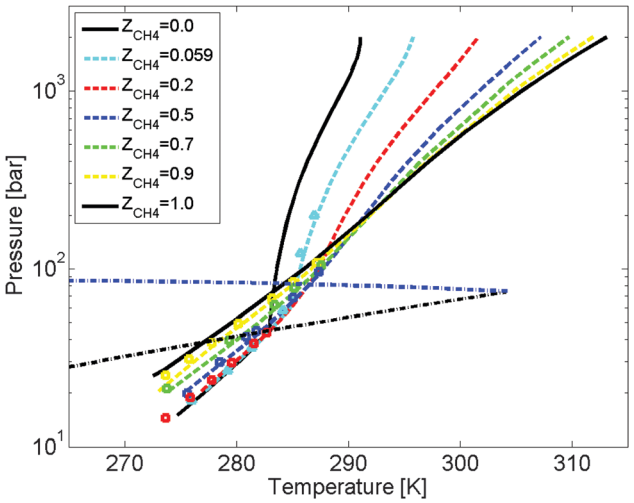

Fig. 1 Phase diagram (*P vs. T*) of the ternary methane–carbon dioxide–water hydrate system. Experimental data (points) and CSMGem calculations (solid lines for binary systems and dashed lines for the ternary system). The black dash-dotted line is the vapor pressure of pure carbon dioxide, while the blue dash-dotted line represents the upper critical end points of the binary carbon dioxide–methane mixture.

and performed MD simulations with the SAFT-γ Mie coarse-grained model. Bruusgaard *et al.*[43] reported experimental solubility measurements, for the particular hydrate system, under three-phase equilibrium conditions (hydrate–liquid–vapor) for pressures lower than 41 bar.

Fig. 1 shows a schematic representation of the three-phase (hydrate–liquid water–guest mixture) equilibrium conditions of the ternary hydrate system for various gas-mixture compositions. The depicted lines denote calculations performed with the CSMGem simulator, which uses the Gibbs energy minimization approach and combines a cubic equation of state with the van der Waals–Platteeuw model in order to calculate the three-phase equilibrium conditions. Further details can be found in ref. 1 and 56. The points show a limited number of characteristic experimental measurements, indicative of the range of conditions where experimental data are available. The solid lines correspond to the cases of either pure methane or pure carbon dioxide hydrate, while the dashed lines correspond to the ternary system for different guest-mixture compositions. Additionally, the upper critical end-points (UCEP)[57] of the binary carbon dioxide–methane mixture as well as the saturation pressure of carbon dioxide are depicted with the blue and black dash-dotted lines respectively.

As can be seen in Fig. 1, for pressures higher than approximately 200 bar the ternary hydrate equilibrium temperature is lower than that of the pure methane hydrate and additionally the guest-mixture forms a single super-critical phase. For pressures slightly lower than approximately 200 bar and above the UCEP of the carbon dioxide–methane mixture, the ternary hydrate equilibrium temperatures can be higher than that of pure methane hydrate. Right below the UCEP it has been shown experimentally that the guest mixture forms a two-phase system, while the ternary mixture is at VLLE state.[51] Finally, in the lower pressure range, the guest-mixture is found in the vapor phase with very low density.

This phase diagram is helpful for the selection of the simulation conditions that are appropriate for the use of the direct phase coexistence methodology, given two significant limitations of the method from our perspective. Firstly, it is not clear to us how the methodology can be used practically for systems with more than three coexisting phases, given that it is necessary from a practical point of view for phases to be in contact with each other. Secondly, performing simulations under the conditions of very low guest-mixture density is highly impractical, as it is then necessary to use an extremely large simulation box to accommodate the guest-rich phase (of the order of 60 nm or more) which creates problems in the pressure coupling and additionally reduces considerably the computational speed. For the aforementioned reasons we have chosen to carry our simulations for pressures higher than 200 bar, as in this area we avoid having a low density guest-rich phase or a guest-mixture forming two phases and also the methane hydrate phase which we use in our initial configuration is thermodynamically stable, as explained in more detail in the next section.

In the case of the ternary hydrate system, there are three important issues to be addressed. Firstly, it is necessary to explore whether the combination of the aforementioned force-fields can be used in a predictive manner for the determination of the three-phase equilibrium conditions, without any further modifications. Secondly, it is essential to understand how the interactions between the molecules of the different guests come into play as they can affect both the solubility in the aqueous phase and the hydrate equilibrium conditions. The final important issue is the examination of the capability of the direct-phase coexistence methodology to handle such a ternary hydrate system.

The paper is organized as follows: initially, the details of the methodology used are presented, including the preparation of structures and implemented force fields. Next, the results are presented and discussed, and finally, the conclusions are summarized.

2. Methodology

For the determination of the three-phase coexistence equilibrium conditions of the ternary hydrate system the direct phase coexistence method was used.[20] In this methodology, we allow three different phases to coexist in our simulation box, namely a solid hydrate phase, a liquid water phase and a guest-rich phase. MD simulations were carried out in the isobaric–isothermal ensemble (*NPT*) at different temperatures in order to identify the equilibrium temperature for a given pressure and composition. Depending on the particular conditions, the hydrate phase can either grow or dissociate, and thus the three-phase equilibrium temperature (T_3) can be identified as the average value between the highest temperature at which hydrate growth occurs and the lowest temperature at which hydrate dissociation takes place. In order to treat the stochastic behavior of the system, which is described in more detail in our previous work,[18] at each pressure four independent temperature scans were carried out and the reported T_3 is the arithmetically averaged value of the four T_3 values calculated for each pressure.

The initial three-phase configuration consists of a methane hydrate slab surrounded by two liquid water slabs which are in contact with the mixed guest-rich phase, resulting in a four slab configuration ordered as water–hydrate–water–guest (WHWG). The guest-rich phase consists of methane and carbon dioxide. It is necessary to have the hydrate slab in direct contact with water due to the very low solubility of water in the guest-rich phase. Hydrate growth would be practically impossible if the hydrate phase were to be in contact with the guest-rich phase only.

The selection of the initial hydrate phase to be that of a methane hydrate is based on three reasons. The first one is that methane hydrate has the same sI structure as the mixed carbon dioxide–methane hydrate,[1] and so it can serve as a suitable growth substrate. The second reason is that, in the range of pressures studied in this work, the three-phase coexistence temperatures of the mixed hydrate are higher than that of pure carbon dioxide and lower than that of pure methane hydrate. Although carbon dioxide hydrate has also the sI structure, the methane hydrate is more stable than carbon dioxide hydrate under the conditions examined. The third and most important reason is that it is unclear to us what should be the correct partial fractions of carbon dioxide and methane in the mixed hydrate phase. Even with the knowledge of this information, our study, as it is shown later, indicates that the distribution of the two guest molecules in the mixed hydrate phase is to a certain extent random.

The dimensions of the hydrate slab correspond to that of a $2 \times 2 \times 2$ sI hydrate supercell. The positions of the oxygen atoms in the unit cell of the sI methane hydrate were obtained from XRD data as reported by McMullan and Jeffrey.[58] The hydrogen atoms are initially randomly positioned around each oxygen atom, respecting the geometry of the water forcefield, and their final positions are found by energy minimization, using the steepest descent algorithm, resulting in a structure that obeys the Bernal and Fowler rules.[59] It has been shown[60] that this approach is an alternative to that of dipole moment minimization. The methane molecules are placed in the center of the cages with 100% occupancy. Thus, the initial structure has 368 water and 64 methane molecules.

Following a short equilibration of the hydrate slab at each pressure and temperature, the water and methane–carbon dioxide slabs are constructed with their tangential dimensions equal to that of the hydrate slab. After equilibration of each slab, the four slabs are connected with a 0.1 nm buffer distance, followed by energy minimization to avoid overlaps, while keeping the oxygen positions frozen. Each water slab consists of 368 molecules while the methane–carbon dioxide slab consists of 400 molecules in total.

The three-phase equilibrium temperature was calculated at three different pressures, namely 400, 1000 and 2000 bar. Given that T_3 depends on the composition, we also investigated two compositions, where the initially prepared methane–carbon dioxide slab consisted of a methane mole fraction of 0.5 and 0.2, respectively.

Table 1 Forcefield parameters for TIP4P/ice (water),[22] OPLS-UA (methane),[26] and TraPPE (carbon dioxide).[28] The distance between atoms A and B is denoted by d_{AB}. The angle, in degrees, formed at the central atom B separating two A atoms is denoted by ∠A–B–A. The Lennard-Jones parameters are denoted by σ (size parameter) and ε/k_B (energy parameter), with k_B the Boltzmann constant. The charge is denoted by q

Force field	Atom	σ (Å)	ε/k_B (K)	q (e)	Geometry	
TIP4P/ice water	O	3.1668	106.1	0.0	d_{OH} (Å)	0.9572
	H	0.0	0.0	0.5897	∠H–O–H	104.5
	M	0.0	0.0	−1.1794	d_{OM} (Å)	0.1577
OPLS-UA methane	CH_4	3.73	148	0.0		
TraPPE carbon dioxide	C	2.800	27.0	0.700	d_{CO} (Å)	1.16
	O	3.050	79.0	−0.350	∠O–C–O	180

The rigid, non-polarizable models TIP4P/ice,[24] OPLS-UA[26] and TraPPE[28] were used to describe water, methane and carbon dioxide respectively. The parameters for these models are given in Table 1. It should be noted that the OPLS-UA methane model is practically the same as the TraPPE methane model, so effectively, both guest molecules can be described by the TraPPE forcefield. The Lorentz–Berthelot[16] combining rules were used for the Lennard-Jones cross-interaction parameters. Consistent with our previous work,[19] the cross-interaction energy parameter between the oxygen of water and the oxygens of carbon dioxide was modified by a factor of χ = 1.08, according to the equation

$$\varepsilon_{O(CO_2)-O(H_2O)} = \chi\sqrt{\varepsilon_{O(CO_2)}\varepsilon_{O(H_2O)}} \quad (1)$$

where $\varepsilon_{O(CO_2)}$ and $\varepsilon_{O(H_2O)}$ are the Lennard-Jones energy parameters for oxygen in carbon dioxide and water, respectively. This modification was found necessary in order to correct the predicted solubility of carbon dioxide in the aqueous phase, which consequently corrects the predicted T_3 of the pure carbon dioxide hydrate system in the whole range of pressures above the quadruple point up to 5000 bar.

The GROMACS MD simulation package (version 4.6.5)[61–63] was used and all simulations were carried out in the isobaric–isothermal ensemble (*NPT*). The Berendsen[64] temperature and pressure coupling schemes were employed with time constants of 1 ps. Anisotropic pressure coupling was used for the WHWG system with equal compressibility in all directions, so that each dimension can fluctuate independently, in order to avoid inducing stresses to the hydrate crystal. The leap-frog integration algorithm was employed with a time step of 2 fs and periodic boundary conditions were applied in all directions. The Lennard-Jones potential was truncated at 11 Å without employing any dispersion corrections as the system is anisotropic and inhomogeneous. The long range Coulombic interactions were handled with the particle mesh Ewald (PME) method.[65] Four independent temperature scans were performed at each pressure by using different initial velocities. It should be noted that in order to allow for a clear conclusion about the evolution of the system to that of either hydrate growth or dissociation, it is necessary that the simulations are more than 2000 ns long, rendering this type of calculations computationally demanding.

For the calculation of the solubility of the guest molecules in the liquid water-rich phase, direct phase coexistence MD simulations were carried out using a two-slab configuration, one for the water and one for the guest phase. The water slab contained 1104 molecules while the guest slab contained 400 molecules. During these calculations the tangential to the interface dimensions were kept fixed and equal to 2.4 nm which also corresponds to the dimensions of the cubic hydrate slab. The solubility was calculated with a 2 ns block-averaging scheme over a 200 ns long trajectory.

3. Results and discussion

In our previous studies we have demonstrated that the combinations of TIP4P/ice–OPLS-UA for the water–methane system, and the modified TIP4P/ice–TraPPE for the water–carbon dioxide system provide good predictions of the guest solubility in the water-rich phase under hydrate equilibrium conditions. In the present study the main focus is the examination of how well-behaved is the combination of these forcefields for the ternary system with respect to the predictions of the three-phase equilibrium temperature T_3. Given the important effect of solubility on the accuracy of the T_3 predictions, we have calculated the solubility of both guests in the water-rich phase under the three-phase equilibrium conditions. The results are presented in Fig. 2 along with comparison with the solubility predicted by CSMGem, given the lack of experimental solubility data under hydrate equilibrium conditions in this region. For each pressure the corresponding temperature is equal to the three-phase equilibrium temperature as predicted by CSMGem. An equimolar initial feed composition of the methane–carbon dioxide mixture was used in these simulations, but the final equilibrium bulk composition of the guest-rich phase corresponds to a value of 0.6 methane mole fraction. This is due to the different solubility of the two species in the aqueous phase and primarily due to the strong adsorption of the carbon dioxide molecules on the water interface, so that the initial load is always significantly different from the equilibrium composition. Naturally, this is also true for the case of the ternary hydrate system, where although the initial compositions were 0.5 and 0.2 methane mole fraction in the guest-mixture, the equilibrium methane mole fraction in the guest-rich phase was calculated to be 0.6 and 0.25, respectively. The strong adsorption of carbon dioxide on the water interface has been previously reported in various studies.[66–68] The MD-calculated solubility agrees, within the computational standard deviation, with the predictions of CSMGem for both carbon dioxide and methane, although it appears that the slopes are slightly different.

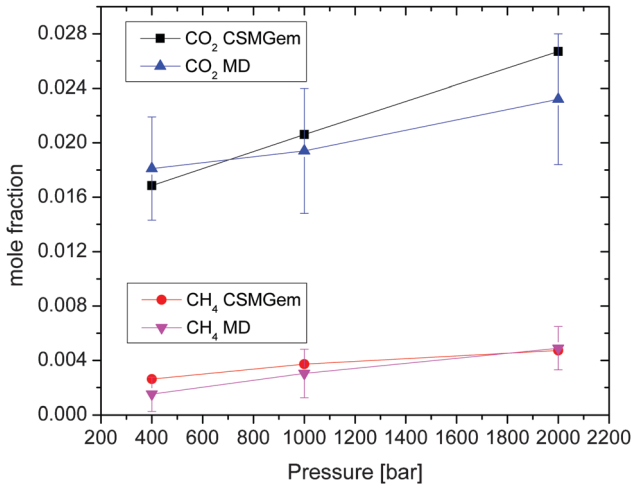

Fig. 2 Carbon dioxide and methane solubility in the aqueous phase (mole fraction) as a function of the three-phase equilibrium pressure. Comparison between MD and CSMGem results. The equilibrium temperatures calculated by CSMGem (0.6 methane mole fraction) for 400, 1000, and 2000 bar are 295.9, 302.6, and 308.5 K respectively. Lines are guides to the eye only.

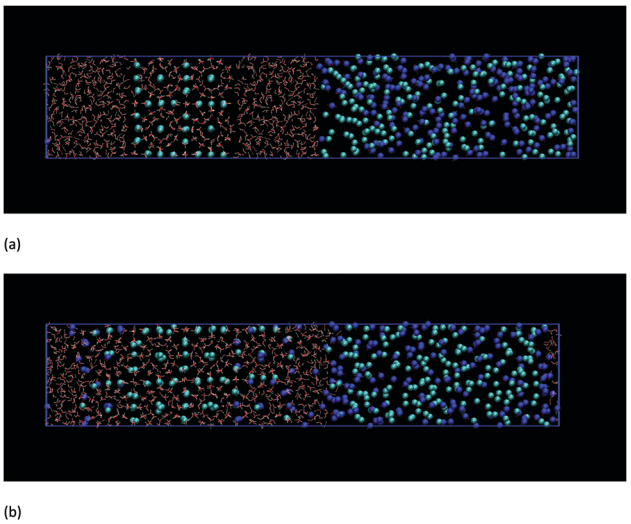

Fig. 4 Two snapshots of a typical MD trajectory of the ternary hydrate system at 400 bar and 291.4 K: (a) initial configuration and (b) final state. Dark blue spheres correspond to the carbon atom of the carbon dioxide molecule, light blue spheres correspond to methane molecules, and red and white lines represent the water molecules.

Ghafri *et al.*[51] have determined experimentally the solubility in the aqueous phase of the VLE ternary system at 100 bar and 323.15 K which is the experimental data with the closest available temperature to the hydrate equilibrium conditions of interest. Comparison of the MD results with this experimental measurement is presented in Fig. 3 along with the dependence of carbon dioxide and methane solubility on the methane mole fraction in the guest-rich phase (methane–carbon dioxide). The agreement is satisfactory as is also the agreement with the solubility in the aqueous phase given by the models of Duan *et al.*[69] and Sun and Duan[70] for the binary systems, also presented in Fig. 3. Thus, the combination of these particular forcefields can predict correctly the solubility of both gases in the aqueous phase close to the hydrate equilibrium conditions. Additionally, the solubility of each guest decreases by the addition of the other guest, a conclusion which is in disagreement with the conclusions drawn by Qin *et al.*[54] and Ghafri *et al.*[51]

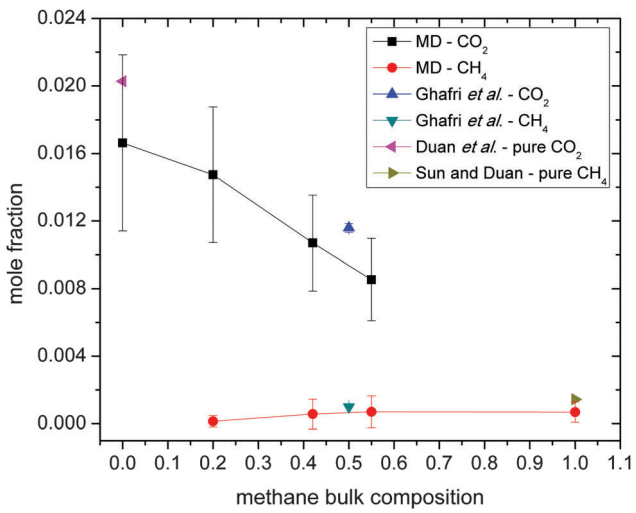

Fig. 3 MD predicted solubility of carbon dioxide and methane in the aqueous phase as a function of the methane composition in the guest-rich phase, at 100 bar and 323.15 K. Comparison with experimental measurements by Ghafri *et al.*[51] and the results of the models by Duan *et al.*[69] and Sun and Duan[70] for the respective binary mixtures.

Fig. 4 presents two indicative snapshots of a typical trajectory used in the determination of the three-phase coexistence conditions. The first snapshot (Fig. 4a) depicts the initial four-slab configuration of the system, while the second snapshot (Fig. 4b) represents the final state, where hydrate growth has taken place given the favorable conditions in this particular example (400 bar and 291.4 K). An example of a single temperature scan is given in Fig. 5 where the time evolution of the potential energy of the system is presented for four different temperatures at 400 bar and for a methane mole fraction in the guest-rich phase of 0.6. In this particular case, the prediction by CSMGem is T_3 = 295.9 K. If both CSMGem and our method are accurate, one would expect to estimate from MD a value of T_3 = 292.9 K, given the $\Delta T = -3$ K deviation caused by the use of TIP4P/ice forcefield. At T = 291.4 K hydrate growth takes place, at T = 297.4 K the potential energy evolution is indicative of hydrate dissociation, and for T = 293.4 K and T = 295.4 K the system remains stable. In this case the MD T_3 value cannot be calculated as the average value between the highest temperature at which hydrate growth occurs (291.4 K) and the lowest temperature at which hydrate melting dissociation takes place (297.4 K). This is because in our system the hydrate phase is composed of methane hydrate whose MD expected T_3 = 294.2 K, so within statistical uncertainty the system is expected to remain stable in the range of T = 292.9 K to T = 294.2 K. Thus, T_3 must be calculated as the average between the maximum temperature at which growth takes place and the minimum temperature at which the system remains stable. In this case this

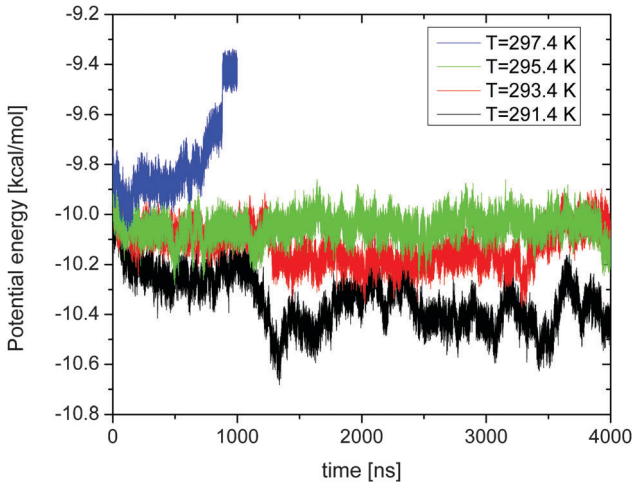

Fig. 5 Indicative time evolution of the potential energy of the ternary hydrate system at 400 bar and for four different temperatures close to the equilibrium T_3.

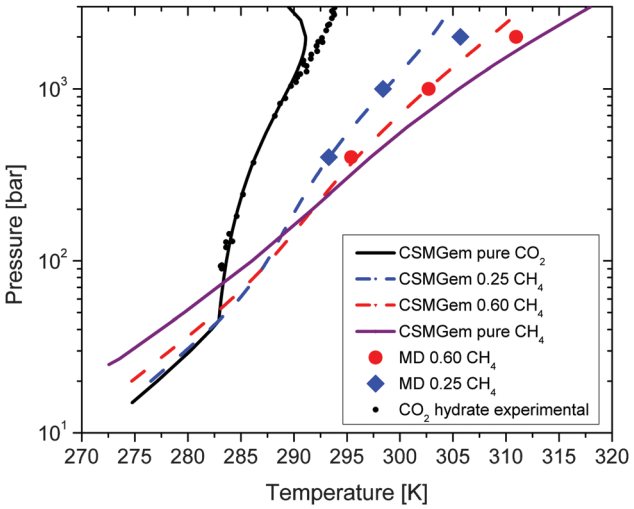

Fig. 6 MD results for the three-phase coexistence conditions of the ternary hydrate system for two methane bulk compositions (0.6 red circles and 0.25 blue diamonds). Comparison with the respective CSMGem predictions (red and blue dashed lines). The three-phase coexistence lines for the binary hydrate systems (solid lines) as predicted by CSMGem are also presented. Small black circles correspond to carbon dioxide hydrate experimental data[1,71,72] for pressures higher than approximately 100 bar.

corresponds to a value of 292.4 K which is very close to the expected value of 292.9 K. As mentioned before, four independent temperature scans per pressure are carried out in order to calculate the reported MD T_3 values.

The predicted three-phase equilibrium temperatures are presented in Table 2 for 400, 1000, and 2000 bar, and for two methane compositions in the guest-rich phase, namely 0.6 and 0.25 mole fraction (starting from an initial load mole fraction of 0.5 and 0.2, respectively). These results are also presented in Fig. 6, corrected by +3 K, so that they can be directly compared with the CSMGem predictions, given that the MD method is known to include a −3 K error that is caused by the use of the TIP4P/ice water model which underpredicts the melting temperature of ice by 3 K.[18,19,22] We observe that for both compositions the agreement between the MD results and CSMGem is satisfactory up to 1000 bar, while deviations appear at higher pressures. It should be noted, however, that the predictions of CSMGem for the case of pure carbon dioxide hydrate deviate from experimental data[1,71,72] for pressures higher than 1000 bar, as shown in Fig. 6, while our methodology can consistently predict T_3 up to 5000 bar.[19] Thus, it is possible that the inefficiency of CSMGem to describe accurately the high pressure retrograde behavior of the carbon dioxide hydrate system is also reflected in the case of the ternary hydrate system.

During the MD simulations, while the total number of molecules in the three-phase system is conserved, since no molecules are added or removed, the total number of molecules in each phase can change, due to hydrate formation/dissociation. Thus, the fact that our finite-sized system is closed affects the determination of T_3 as during the simulation the composition in the guest-rich phase dynamically changes, causing a shift in T_3, with respect to the value of T_3 that corresponds to a given initial composition. Nevertheless, due to the finite character of our system it is possible to estimate this shift in T_3 having as a guide the dependence of T_3 on composition as predicted by CSMGem. This calculation, however, depends also on the relative composition of the guest molecules in the hydrate phase, denoted thereby as the guest hydrate fraction, expressing the ratio of guest molecules of a particular species over the sum of all guest molecules in the hydrate phase. In Fig. 7, indicative results are presented, where the shift in T_3 is given as a function of the number of new hydrate unit cells that have been added to the crystal, for the case of 400 bar, the equimolar guest-phase composition and as a function of the carbon dioxide hydrate fraction. For the given system size of our simulations, the maximum number of hydrate unit cells that can be added is 16, and thus the shift in T_3 is of the order of 0.5 K for values of the carbon dioxide hydrate fraction in the range of 0.4–0.6, which as shown later are quite reasonable. For a pressure of 2000 bar the maximum shift in T_3 is approximately 1 K. In this way, it is shown that the correction that should be applied to the estimation of T_3 from MD simulations with a closed system, with the implication of dynamically varying guest-rich phase composition, is rather small and of the same order of magnitude as the uncertainty that is inherent to this methodology, and thus this correction for this particular case can be ignored.

An estimation of the guest hydrate fraction can be obtained from the MD simulations by measuring it directly in the grown

Table 2 MD results for the three-phase coexistence temperature T_3 [K] of the ternary hydrate system at 400, 1000, and 2000 bar, and for 0.6 and 0.25 methane mole fraction in the guest-rich phase. The statistical uncertainty in temperature is given in parentheses

	Temperature [K]	
Pressure [bar]	Methane mole fraction 0.6	Methane mole fraction 0.25
400	292.4 (0.0)	290.3 (1.2)
1000	299.7 (1.2)	295.4 (1.2)
2000	307.9 (0.5)	302.7 (0.0)

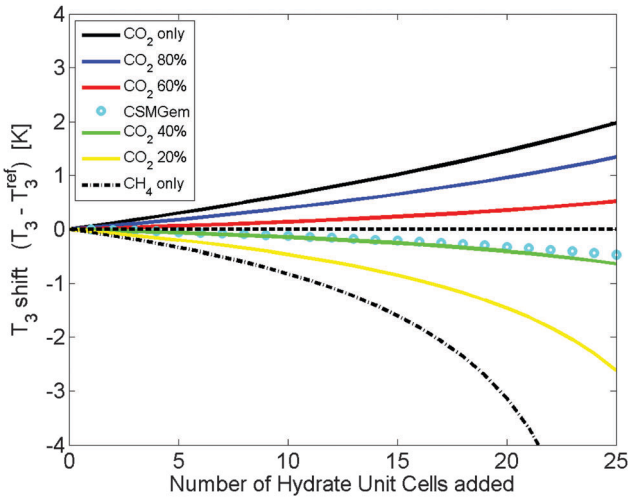

Fig. 7 Shift of T_3 due to the use of a finite-sized closed system, for an initial methane bulk mole fraction of 0.5 at 400 bar, as a function of hydrate growth (expressed in terms of sI unit cells) and the carbon dioxide hydrate fraction. The reference temperature T_3^{ref} corresponds to the equilibrium T_3 for the initial 0.5 methane mole fraction.

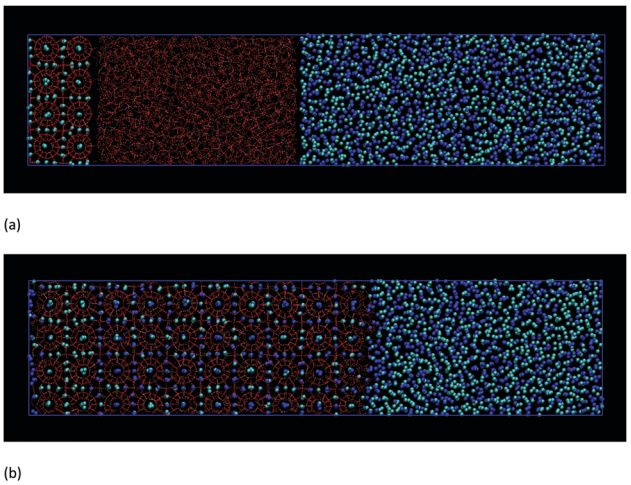

Fig. 8 Initial (a) and final (b) configurations of the MD simulation used in the estimation of the carbon dioxide hydrate fraction, at 2000 bar and 295 K. Dark blue spheres correspond to the carbon atom of the carbon dioxide molecule, light blue spheres correspond to methane molecules, and red lines represent the hydrogen bonds between the water molecules.

part of the hydrate phase. Our simulations (using the 2 × 2 × 2 initial hydrate configuration) indicate that the carbon dioxide hydrate fraction is approximately 0.6 for both guest-rich phase compositions and for all three pressures examined. Nevertheless, due to the small size of our ternary simulation system, the newly grown hydrate part was not big enough to provide a clear picture of the carbon dioxide hydrate fraction. For this reason we estimated this fraction in a larger system, which consists of a 4 × 2 × 2 unit cell methane hydrate phase in contact with a water phase with 3000 molecules and a guest phase with 1000 carbon dioxide and 1000 methane molecules. Given the high computational cost and taking into consideration the growth rate of the hydrate, we chose 2000 bar and 295 K to be the conditions of this simulation. The initial and the final state of this system are presented in Fig. 8, where in snapshot (a) the three initial phases are shown, while in snapshot (b) the hydrate phase has grown by 8 × 2 × 2 unit cells, as much as the water content allowed. In Fig. 9 the ratio of carbon dioxide molecules over the sum of the molecules of both guests is given as a function of the box length for the final state of the system, which corresponds to Fig. 8b. On the left, in the area of approximately 0–2.5 nm this ratio is zero corresponding to the initial methane hydrate slab. The part in the range of 2.5–12 nm corresponds to the newly formed mixed hydrate phase and finally the last part on the right corresponds to the guest-rich phase. As mentioned before, although the initial load was 0.5 methane mole fraction, the equilibrium guest-rich phase composition, for the whole duration of the simulation, is closer to 0.6 methane mole fraction. The carbon dioxide hydrate fraction, as given directly by the middle part of Fig. 9, has an average value of 0.56, and exhibits fluctuations.

Yi *et al.*,[29] in their MD study, also observed a high carbon dioxide hydrate fraction, however not under comparable conditions and using a highly supersaturated solution. Contrary to these MD results, CSMGem for 0.6 methane mole fraction of the

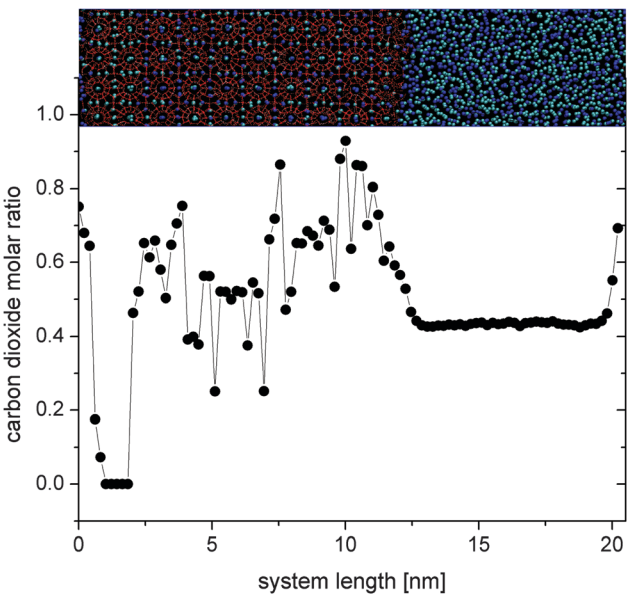

Fig. 9 Ratio of carbon dioxide molecules over the sum of the molecules of both guests as a function of the box length for the final state of the large ternary hydrate system, at 2000 bar and 295 K, corresponding to Fig. 8b.

guest-rich phase, at 2000 bar and 308.3 K, the respective predicted equilibrium temperature, predicts a value of 0.24 for the carbon dioxide hydrate fraction.

The guest hydrate fraction, in general, is not a quantity that can be either easily or very accurately measured experimentally. In general, two types of experiments have been reported. Studies of the first type performed analysis (*e.g.*, Raman) in order to identify which types of guests are enclathrated inside the different types of cages within a hydrate structure.[73–77] On the other hand, studies of the second type performed analysis of the relative amount of gas that is released from the dissociation of formed hydrates.[78–83]

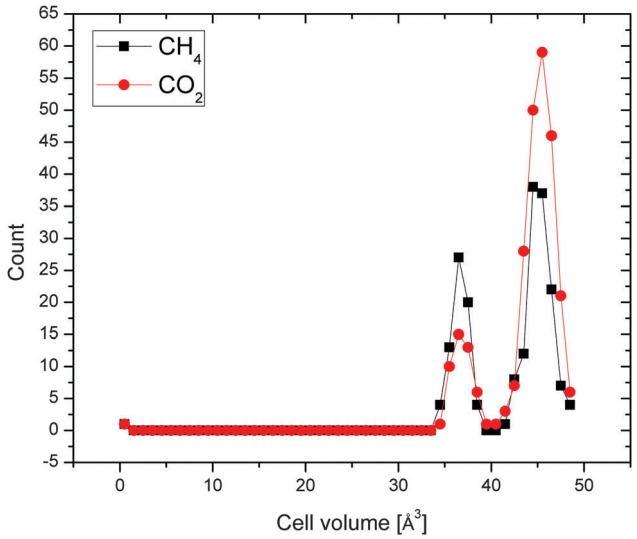

Fig. 10 Distribution of volumes of Voronoi cells for methane and carbon dioxide guests in the grown mixed hydrate phase at 2000 bar and 295 K.

These studies were primarily interested in calculating the separation efficiencies of gas mixtures with the use of hydrates. In the region of interest to this study there are no experimental measurements available as the aforementioned experimental works are for pressures below 50 bar. An exception is the study by Nakano and Ohgaki[74] which reported no change in the composition between the initial gas feed and the gas resulting after hydrate dissociation for the case of hydrate formation at 1000 bar.

It is noteworthy that in our MD simulations, as is also evident from Fig. 8b, the small 5^{12} cages can be occupied, apart from methane molecules, by carbon dioxide molecules as well, although to a smaller extent. To further elucidate this point quantitatively, we carried out on the grown mixed hydrate of the final state of the simulation at 2000 bar and 295 K (see Fig. 8b) an analysis based on Voronoi tessellation[84] which was able to identify the distribution of the occupancies of the methane and carbon dioxide guests in the small and large cages. The analysis was carried out using radical Voronoi tessellation as implemented in Voro++[85] where the radii of the atoms were taken into account in space tessellation. The result is presented in Fig. 10, where for each guest two distinct peaks can be identified with direct correspondence to the small and large cages. Based on this information we calculated that the molar fraction of carbon dioxide in the small cages is 0.40 while in the large cages it is 0.63. The respective values predicted by CSMGem at 2000 bar and the equilibrium temperature of 308.5 K are 0.041 and 0.308. This finding by MD is in agreement with the experimental observations reported by Nakano and Ohgaki,[74] Lee *et al.*,[75] and Everett *et al.*[76] On the other hand, the work of Sum *et al.*[73] reported the presence of methane-only in the small cages. The MD simulations indicate that the presence of carbon dioxide molecules is prevalent in the larger $5^{12}6^2$ cages. This observation is also in agreement with experimental observations reported by Everett *et al.*,[76] Sum *et al.*,[73] and Kang *et al.*[77]

4. Conclusions

The direct phase coexistence methodology was implemented for the determination of the three-phase coexistence conditions of a ternary hydrate system, namely methane–carbon dioxide–water. The three-phase coexistence temperature was determined at 400, 1000 and 2000 bar and for two methane compositions of the guest-rich phase, 0.6 and 0.25 mole fraction. The results, due to lack of experimental data in this region, were compared with predictions by CSMGem. For both compositions examined, agreement was observed up to 1000 bar while deviations exist for higher pressures. The stochastic behavior that is inherent to these systems was taken into consideration through statistical averaging of multiple MD realizations. Additionally, the dynamically varying composition of the guest-rich phase, which is characteristic for a finite-sized closed ternary system, was taken into consideration and it was shown that it does not affect significantly the calculated T_3. Furthermore, the relative ratio of the guest molecules in the mixed hydrate phase was estimated, showing a higher occupancy for the carbon dioxide molecules. Additionally, the carbon dioxide molecules were found to occupy the smaller cages of the sI structure as well, but to a lesser degree than the methane molecules, consistent with reported experimental observations.

The use of the TIP4P/ice water model introduces for this ternary system an underprediction of T_3 by 3 K, similarly to the case of the binary systems, and equal to the deviation of this model for the prediction of the melting temperature of ice. Furthermore, the solubility of the guest molecules in the aqueous phase was calculated and was found to be in good agreement with existing data. The addition of methane was found to reduce the solubility of carbon dioxide as well as the addition of carbon dioxide reduces the solubility of methane. In general, the combination of the guest forcefields, which were successfully used for the case of the binary hydrate systems in our earlier studies,[18,19] was shown to be adequate for the description of the ternary system. This is reflected by the accurate calculation of the guest solubility in the water-rich phase and the calculated three-phase coexistence conditions of the ternary hydrate system.

Acknowledgements

This publication was made possible by NPRP Grant No. 6-1547-2-632 from the Qatar National Research fund (a member of the Qatar Foundation). The statements made herein are solely the responsibility of the authors. We are grateful to the High Performance Computing Center of Texas A&M University at Qatar for generous resource allocation. The contribution of Dr. Loukas D. Peristeras in the calculations based on Voronoi tessellation is also gratefully acknowledged.

References

1 E. D. Sloan and C. A. Koh, *Clathrate Hydrates of Natural Gases*, CRC Press, Taylor & Francis Group, New York, 3rd edn, 2008.
2 J. S. Loveday and R. J. Nelmes, High-pressure gas hydrates, *Phys. Chem. Chem. Phys.*, 2008, **10**(7), 937–950.

3 L. E. Zerpa, J.-L. Salager, C. A. Koh, E. D. Sloan and A. K. Sum, Surface chemistry and gas hydrates in flow assurance, *Ind. Eng. Chem. Res.*, 2011, **50**, 188–197.

4 M. A. Kelland, History of the development of low dosage hydrate inhibitors, *Energy Fuels*, 2006, **20**, 825–847.

5 R. Boswell and T. S. Collett, Current perspectives on gas hydrate resources, *Energy Environ. Sci.*, 2011, **4**, 1206–1215.

6 H. P. Veluswamy, R. Kumar and P. Linga, Hydrogen storage in clathrate hydrates: Current state of the art and future directions, *Appl. Energy*, 2014, **122**, 112–132.

7 S. Thomas and R. A. Dawe, Review of ways to transport natural gas energy from countries which do not need the gas for domestic use, *Energy*, 2003, **28**, 1461–1477.

8 P. Babu, P. Linga, R. Kumar and P. Englezos, A review of the hydrate based gas separation (HBGS) process for carbon dioxide pre combustion capture, *Energy*, 2015, **85**, 261–279.

9 F. M. O'Connor, O. Boucher, N. Gedney, C. D. Jones, G. A. Folberth, R. Coppell, P. Friedlingstein, W. J. Collins, J. Chappellaz, J. Ridley and C. E. Johnson, Possible role of wetlands, permafrost, and methane hydrates in the methane cycle under future climate change: a review, *Rev. Geophys.*, 2010, **48**, RG4005.

10 M. Vanneste, N. Sultan, S. Garziglia, C. F. Forsberg and J.-S. L'Heureux, Seafloor instabilities and sediment deformation processes: the need for integrated, multi-disciplinary investigations, *Mar. Geol.*, 2014, **352**, 183–214.

11 D. R. McConnell, Z. Zhang and R. Boswell, Review of progress in evaluating gas hydrate drilling hazards, *Mar. Pet. Geol.*, 2012, **34**, 209–223.

12 A. Eslamimanesh, A. H. Mohammadi, D. Richon, P. Naidoo and D. Ramjugernath, Application of gas hydrate formation in separation processes: a review of experimental studies, *J. Chem. Thermodyn.*, 2012, **46**, 62–71.

13 G. D. Holder, S. P. Zetts and N. Pradhan, Phase behavior in systems containing clathrate hydrates: a review, *Rev. Chem. Eng.*, 1988, **5**, 1–70.

14 Z. Duan and R. Sun, A model to predict phase equilibrium of CH_4 and CO_2 clathrate hydrate in aqueous electrolyte solutions, *Am. Mineral.*, 2006, **91**, 1346–1354.

15 S. El Meragawi, N. I. Diamantonis, I. N. Tsimpanogiannis and I. G. Economou, Hydrate – fluid phase equilibria modeling using PC-SAFT and Peng-Robinson equations of state, *Fluid Phase Equilib.*, 2016, **413**, 209–219.

16 D. Frenkel and B. Smit, *Understanding Molecular Simulation: From Algorithms to Applications*, Academic Press, San Diego, California, USA, 2nd edn, 2002.

17 N. J. English and J. M. D. MacElroy, Perspectives on molecular simulation of clathrate hydrates: progress, prospects and challenges, *Chem. Eng. Sci.*, 2015, **121**, 133–156.

18 V. K. Michalis, J. Costandy, I. N. Tsimpanogiannis, A. K. Stubos and I. G. Economou, Prediction of the phase equilibria of methane hydrates using the direct phase coexistence methodology, *J. Chem. Phys.*, 2015, **142**, 044501.

19 J. Costandy, V. K. Michalis, I. N. Tsimpanogiannis, A. K. Stubos and I. G. Economou, The role of intermolecular interactions in the prediction of the phase equilibria of carbon dioxide hydrates, *J. Chem. Phys.*, 2015, **143**, 094506.

20 A. J. C. Ladd and L. V. Woodcock, Triple-point coexistence properties of the Lennard-Jones system, *Chem. Phys. Lett.*, 1977, **51**, 155–159.

21 J. R. Espinosa, E. Sanz, C. Valeriani and C. Vega, On fluid-solid direct coexistence simulations: the pseudo-hard sphere model, *J. Chem. Phys.*, 2013, **139**, 144502.

22 M. M. Conde and C. Vega, Determining the three-phase coexistence line in methane hydrates using computer simulations, *J. Chem. Phys.*, 2010, **133**, 064507.

23 J. M. Míguez, M. M. Conde, J.-P. Torré, F. J. Blas, M. M. Piñeiro and C. Vega, Molecular dynamics simulation of CO_2 hydrates: Prediction of three phase coexistence line, *J. Chem. Phys.*, 2015, **142**, 124505.

24 J. L. F. Abascal, E. Sanz, R. García Fernández and C. Vega, A potential model for the study of ices and amorphous water: TIP4P/Ice, *J. Chem. Phys.*, 2005, **122**, 234511.

25 R. García Fernández, J. L. F. Abascal and C. Vega, The melting point of ice Ih for common water models calculated from direct coexistence of the solid–liquid interface, *J. Chem. Phys.*, 2006, **124**, 144506.

26 W. L. Jorgensen, J. D. Madura and C. J. Swenson, Optimized Intermolecular Potential Functions for Liquid Hydrocarbons, *J. Am. Chem. Soc.*, 1984, **106**, 6638.

27 H. Docherty, A. Galindo, C. Vega and E. Sanz, A potential model for methane in water describing correctly the solubility of the gas and the properties of the methane hydrate, *J. Chem. Phys.*, 2006, **125**, 074510.

28 J. J. Potoff and J. I. Siepmann, Vapor–liquid equilibria of mixtures containing alkanes, carbon dioxide, and nitrogen, *AIChE J.*, 2001, **47**, 1676–1682.

29 L. Yi, D. Liang, X. Zhou and D. Li, Molecular dynamics simulations for the growth of CH_4–CO_2 mixed hydrate, *J. Energy Chem.*, 2014, **23**, 747–754.

30 L. Yi, D. Liang, S. Liang and X. Zhou, Molecular dynamics study of CH_4–CO_2 mixed hydrate dissociation, *Asia-Pac. J. Chem. Eng.*, 2015, **10**, 823–832.

31 P. Dornan, S. Alavi and T. K. Woo, Free energies of carbon dioxide sequestration and methane recovery in clathrate hydrates, *J. Chem. Phys.*, 2007, **127**, 124510.

32 Y. Qi, M. Ota and H. Zhang, Molecular dynamics simulation of replacement of CH4 in hydrate with CO_2, *Energy Convers. Manage.*, 2011, **52**, 2682–2687.

33 Y.-T. Tung, L.-J. Chen, Y.-P. Chen and S.-T. Lin, *In situ* methane recovery and carbon dioxide sequestration in methane hydrates: a molecular dynamics simulation study, *J. Phys. Chem. B*, 2011, **115**, 15295–15302.

34 Y. Iwai, H. Nakamura and M. Hirata, Molecular dynamics simulation of replacement of methane hydrate with carbon dioxide, *Mol. Simul.*, 2012, **38**, 481–490.

35 D. Bai, X. Zhang, G. Chen and W. Wang, Replacement mechanism of methane hydrate with carbon dioxide from microsecond molecular dynamics simulations, *Energy Environ. Sci.*, 2012, **5**, 7033–7041.

36 J. Liu, Y. Yan, S. Li, J. Xu, G. Chen and J. Zhang, Structure and stability of binary CH_4–CO_2 clathrate hydrates, *Comput. Theor. Chem.*, 2016, **1086**, 1–6.

37 J. Liu, Y. Yan, H. Liu, J. Xu, J. Zhang and G. Chen, Understanding effect of structure and stability on transformation of CH_4 hydrate to CO_2 hydrate, *Chem. Phys. Lett.*, 2016, **648**, 75–80.

38 X. Wang, D. K. Sang, J. Chen and J. Mi, Theoretical insights into nucleation of CO_2 and CH_4 hydrates for CO_2 capture and storage, *Phys. Chem. Chem. Phys.*, 2014, **16**, 26929–26937.

39 K. S. Glavatskiy, T. J. H. Vlugt and S. Kjelstrup, Toward a possibility to exchange CO_2 and CH_4 in sI clathrate hydrates, *J. Phys. Chem. B*, 2012, **116**, 3745–3753.

40 K. Ohgaki, K. Takano, H. Sangawa, T. Matsubara and S. Nakano, Methane exploitation by carbon dioxide from gas hydrates – phase equilibria for CO_2–CH_4 mixed hydrate system, *J. Chem. Eng. Jpn.*, 1996, **29**, 478–483.

41 H. Komatsu, M. Ota, R. L. Smith and H. Inomata, Review of CO_2–CH_4 clathrate hydrate replacement reaction laboratory studies – properties and kinetics, *J. Taiwan Inst. Chem. Eng.*, 2013, **44**, 517–537.

42 Clathrate Hydrate Physical Property Database, NIST Standard Reference Database # 156, http://gashydrates.nist.gov/.

43 H. Bruusgaard, J. G. Beltrán and P. Servio, Solubility measurements for the CH_4 + CO_2 + H_2O system under hydrate–liquid–vapor equilibrium, *Fluid Phase Equilib.*, 2010, **296**, 106–109.

44 V. Belandria, A. H. Mohammadi and D. Richon, Phase equilibria of clathrate hydrates of methane + carbon dioxide: New experimental data and predictions, *Fluid Phase Equilib.*, 2010, **296**, 60–65.

45 V. Belandria, A. Eslamimanesh, A. H. Mohammadi, P. Théveneau, H. Legendre and D. Richon, Compositional analysis and hydrate dissociation conditions measurements for carbon dioxide + methane + water system, *Ind. Eng. Chem. Res.*, 2011, **50**, 5783–5794.

46 I. B. A. Sfaxi, V. Belandria, A. H. Mohammadi, R. Lugo and D. Richon, Phase equilibria of CO_2 + N_2 and CO_2 + CH_4 clathrate hydrates: Experimental measurements and thermodynamic modeling, *Chem. Eng. Sci.*, 2012, **84**, 602–611.

47 S. Lee, Y. Lee, J. Lee, H. Lee and Y. Seo, Experimental verification of methane–carbon dioxide replacement in natural gas hydrates using a differential scanning calorimeter, *Environ. Sci. Technol.*, 2013, **47**, 13184–13190.

48 Y. Bi, T. Yang and K. Guo, Determination of the upper-quadruple-phase equilibrium region for carbon dioxide and methane mixed gas hydrates, *J. Pet. Sci. Eng.*, 2013, **101**, 62–67.

49 A. Djavidnia, A. A. Izadpanah, M. V. Sefti and F. Varaminian, The equilibrium data and thermodynamic modeling of hydrate formation for CO_2 and mixtures of CO_2 and CH_4 in the presence of methanol, *Pet. Sci. Technol.*, 2013, **31**, 2013–2021.

50 K. M. Sabil, Q. Nasir, B. Partoon and A. A. Seman, Measurement of H-LW-V and dissociation enthalpy of carbon dioxide rich synthetic natural gas mixtures, *J. Chem. Eng. Data*, 2014, **59**, 3502–3509.

51 S. Z. S. Al Ghafri, E. Forte, G. C. Maitland, J. J. Rodriguez-Henríquez and J. P. M. Trusler, Experimental and modeling study of the phase behavior of (methane + CO_2 + water) mixtures, *J. Phys. Chem. B*, 2014, **118**, 14461–14478.

52 A. Eslamimanesh, A. H. Mohammadi and D. Richon, Thermodynamic consistency test for experimental solubility data in carbon dioxide/methane + water system inside and outside gas hydrate formation region, *J. Chem. Eng. Data*, 2011, **56**, 1573–1586.

53 A. Eslamimanesh, S. Babaee, A. H. Mohammadi, J. Javanmardi and D. Richon, Experimental data assessment test for composition of vapor phase in equilibrium with gas hydrate and liquid water for carbon dioxide + methane or nitrogen + water system, *Ind. Eng. Chem. Res.*, 2012, **51**, 3819–3825.

54 J. Qin, R. J. Rosenbauer and Z. Duan, Experimental measurements of vapor–liquid equilibria of the H_2O + CO_2 + CH_4 ternary system, *J. Chem. Eng. Data*, 2008, **53**, 1246–1249.

55 O. Lobanova, A. Mejía, G. Jackson and E. A. Müller, SAFT-γ force field for the simulation of molecular fluids 6: binary and ternary mixtures comprising water, carbon dioxide, and n-alkanes, *J. Chem. Thermodyn.*, 2016, **93**, 320–336.

56 A. L. Ballard and E. D. Sloan Jr., The Next Generation of Hydrate Prediction: An Overview, *J. Supramol. Chem.*, 2002, **2**, 385–392.

57 J. M. Míguez, M. C. dos Ramos, M. M. Pineiro and F. J. Blas, An Examination of the Ternary Methane + Carbon Dioxide + Water Phase Diagram using the SAFT-VR Approach, *J. Phys. Chem. B*, 2011, **115**, 9604–9617.

58 R. K. McMullan and G. A. Jeffrey, Polyhedral clathrate hydrates. IX. Structure of ethylene oxide hydrate, *J. Chem. Phys.*, 1965, **42**, 2725–2731.

59 J. D. Bernal and R. H. Fowler, A theory of water and ionic solution, with particular reference to hydrogen and hydroxyl ions, *J. Chem. Phys.*, 1933, **1**, 515–548.

60 S. Sarupria and P. G. Debenedetti, Molecular Dynamics Study of Carbon Dioxide Hydrate Dissociation, *J. Phys. Chem. A*, 2011, **115**, 6102–6111.

61 D. van der Spoel, E. Lindahl, B. Hess, G. Groenhof, A. E. Mark and H. J. C. Berendsen, GROMACS: Fast, flexible, and free, *J. Comput. Chem.*, 2005, **26**, 1701–1718.

62 B. Hess, C. Kutzner, D. van der Spoel and E. Lindahl, GROMACS 4: algorithms for highly efficient, load-balanced, and scalable molecular simulations, *J. Chem. Theory Comput.*, 2008, **4**, 435–447.

63 S. Pronk, S. Pall, P. Larsson, P. Bjelkmar, R. Apostolov, M. R. Shirts, J. C. Smith, P. M. Kasson, D. van der Spoel, B. Hess and E. Lindahl, GROMACS 4.5: a high-throughput and highly parallel open source molecular simulation toolkit, *Bioinformatics*, 2013, **29**, 845–854.

64 H. J. C. Berendsen, J. P. M. Postma, W. F. van Gunsteren, A. DiNola and J. R. Haak, Molecular dynamics with coupling to an external bath, *J. Chem. Phys.*, 1984, **81**, 3684–3690.

65 U. Essmann, L. Perera, M. L. Berkowitz, T. Darden, H. Lee and L. G. Pedersen, A smooth particle mesh Ewald method, *J. Chem. Phys.*, 1995, **103**, 8577–8593.

66 F. Lehmkuhler, M. Paulus, C. Sternemann, D. Lietz, F. Venturini, C. Gutt and M. Tolan, The Carbon Dioxide–Water Interface at Conditions of Gas Hydrate Formation, *J. Am. Chem. Soc.*, 2009, **131**, 585–589.

67 H. Zhang and S. J. Singer, Analysis of the subcritical carbon dioxide-water interface, *J. Phys. Chem. A*, 2011, **115**, 6285–6296.

68 J. M. Míguez, J. M. Garrido, F. J. Blas, H. Segura, A. Mejía and M. M. Piñeiro, Comprehensive characterization of interfacial behavior for the mixture CO_2 + H_2O + CH_4: comparison between atomistic and coarse grained molecular simulation models and density gradient theory, *J. Phys. Chem. C*, 2014, **118**, 24504–24519.

69 Z. Duan, R. Sun, C. Zhu and I.-M. Chou, An improved model for the calculation of CO_2 solubility in aqueous solutions containing Na^+, K^+, Ca^{2+}, Mg^{2+}, Cl^-, and SO_4^{2-}, *Mar. Chem.*, 2006, **98**, 131–139.

70 R. Sun and Z. Duan, An accurate model to predict the thermodynamic stability of methane hydrate and methane solubility in marine environments, *Chem. Geol.*, 2007, **244**, 248–262.

71 S. Nakano, M. Moritoki and K. Ohgaki, High-pressure phase equilibrium and Raman microprobe spectroscopic studies on the methane hydrate system, *J. Chem. Eng. Data*, 1998, **43**, 807–810.

72 O. Bollengier, M. Choukroun, O. Grasset, E. Le Menn, G. Bellino, Y. Morizet, L. Bezacier, A. Oancea, C. Taffin and G. Tobie, Phase equilibria in the H_2O–CO_2 system between 250–330 K and 0–1.7 GPa: stability of the CO_2 hydrates and H_2O-ice VI at CO_2 saturation, *Geochim. Cosmochim. Acta*, 2013, **119**, 322–339.

73 A. K. Sum, R. C. Burruss and E. D. Sloan Jr., Measurement of clathrate hydrates *via* Raman spectroscopy, *J. Phys. Chem. B*, 1997, **101**, 7371–7377.

74 S. Nakano and K. Ohgaki, Relative cage-occupancy of CO_2–methane mixed hydrate, *J. Chem. Eng. Jpn.*, 2000, **33**, 554–556.

75 Y.-J. Lee, T. Kawamura, Y. Yamamoto and J.-H. Yoon, Phase equilibrium studies of tetrahydrofuran (THF) + CH_4, THF + CO_2, CH_4 + CO_2, and THF + CO_2 + CH_4 hydrates, *J. Chem. Eng. Data*, 2012, **57**, 3543–3548.

76 S. M. Everett, C. J. Rawn, B. C. Chakoumakos, D. J. Keffer, A. Huq and T. J. Phelps, Insights into the structure of mixed CO_2/CH_4 in gas hydrates, *Am. Mineral.*, 2015, **100**, 1203–1208.

77 H. Kang, Y.-H. Ahn, D.-Y. Koh, S. Kim, J. Park and H. Lee, Optical Interpretation of the Chemical Process of CH_4–CO_2 Exchange and Its Application to Gas Hydrate Production, *J. Phys. Chem. C*, 2015, **119**, 21353–21357.

78 J. Tang, D. Zeng, C. Wang, Y. Chen, L. He and N. Cai, Study on the influence of SDS and THF on hydrate-based gas separation performance, *Chem. Eng. Res. Des.*, 2013, **91**, 1777–1782.

79 M. Ricaurte, C. Dicharry, D. Broseta, X. Renaud and J.-P. Torré, CO_2 removal from a CO_2–CH_4 gas mixture by clathrate hydrate formation using THF and SDS as water-soluble hydrate promoters, *Ind. Eng. Chem. Res.*, 2013, **52**, 899–910.

80 B. Castellani, F. Rossi, M. Filipponi and A. Nicolini, Hydrate-based removal of carbon dioxide and hydrogen sulphide from biogas mixtures: experimental investigation and energy evaluations, *Biomass Bioenergy*, 2014, **70**, 330–338.

81 S. Tomita, S. Akatsu and R. Ohmura, Experiments and thermodynamic simulations for continuous separation of CO_2 from CH_4 + CO_2 gas mixture utilizing hydrate formation, *Appl. Energy*, 2015, **146**, 104–110.

82 D.-L. Zhong, Z. Li, Y.-Y. Lu, J.-L. Wang and J. Yan, Evaluation of CO_2 removal from a CO_2 + CH_4 gas mixture using gas hydrate formation in liquid water and THF solutions, *Appl. Energy*, 2015, **158**, 133–141.

83 F. Wang, S. Fu, G. Guo, Z.-Z. Jia, S.-J. Luo and R.-B. Guo, Experimental study on hydrate-based CO_2 removal from CH_4/CO_2 mixture, *Energy*, 2016, **104**, 76–84.

84 A. Okabe, B. Boots, K. Sugihara and S. N. Chiu, *Spatial tessellations: concepts and applications of Voronoi diagrams*, John Wiley & Sons, Inc., New York, NY, 2000.

85 C. H. Rycroft, Voro++: A three-dimensional Voronoi cell library in C++, *Chaos*, 2009, **19**, 041111.

